Journal of Catalysis **199,** 209–216 (2001)
doi:10.1006/jcat.2001.3173, available online at http://www.idealibrary.com on IDEAL®

Oxidation Activity and ^{18}O-Isotope Exchange Behavior of Cu-Stabilized Cubic Zirconia

M. K. Dongare,*,[1] Veda Ramaswamy,* C. S. Gopinath,* A. V. Ramaswamy,* S. Scheurell,† M. Brueckner,† and E. Kemnitz†

*Catalysis Division, National Chemical Laboratory, Pune 411 008, India; and †Institute of Chemistry, Humboldt University, Hessische Straße 1-2, 10115 Berlin, Germany

Received August 1, 2000; revised December 27, 2000; accepted January 11, 2001; published online March 21, 2001

A series of $Cu–ZrO_2$ samples with varying concentrations of Cu from 1 to 33 mol% have been prepared by sol–gel technique and calcined at 873 K. XRD characterization of the samples with a copper content of 2 to 20 mol% reveals the stabilization of zirconia into cubic (fluorite) phase. The $Cu–ZrO_2$ samples with higher Cu content (>20 mol%) revealed the presence of bulk CuO. A linear decrease in lattice parameter with increase in Cu content up to 20 mol% indicates the possible incorporation of Cu^{2+} in the lattice position of Zr^{4+} ions. XPS data of these samples provide further evidence for the incorporation of Cu^{2+} ions in the ZrO_2 lattice up to 5 mol%. At higher concentrations of Cu, about half of the input of Cu goes into the lattice and the remaining stays as extra lattice Cu, possibly on the surface or subsurface layer of ZrO_2. The BET surface area of these samples was in the range of 2 to 8 $m^2\ g^{-1}$. The activity of these samples in CH_4 and CO oxidation was investigated by ^{18}O-isotope exchange as well as by catalytic reaction studies in complete oxidation of CH_4 and CO. The $Cu–ZrO_2$ with 20 mol% Cu was found to be the most active sample in the series, which has the maximum amount of copper in the substitutional position. For comparison, yttrium-stabilized zirconia samples with and without Cu was also prepared following the same procedure. Yttrium-stabilized zirconia without Cu was almost inactive in complete methane oxidation, whereas Cu-containing sample was more active. This confirms that the presence of Cu species in substitutional positions along with oxygen vacancies in zirconia lattice are substantially responsible for the catalytic activity in CH_4 and CO oxidation as well as in complete heterogeneous ^{18}O exchange processes. The light-off temperature for 50% conversion of CH_4 (T_{50}) decreases with an increase in Cu content up to 20 mol% and matches well with the results of ^{18}O exchange measurements. The shapes of the curves of T_{50} and $T_{exchange}$ follow a similar trend indicating that both CH_4 oxidation and ^{18}O exchange processes occur *via* a completely heterogeneous mechanism.

Key Words: **Cu-stabilized zirconia; Cu-zirconia catalyst; cubic zirconia; CH_4 oxidation; methane combustion; ^{18}O isotope exchange; oxygen isotope exchange.**

INTRODUCTION

Zirconium oxide has been widely studied for its applications in advanced ceramics, such as refractories, piezoelectric devices, ceramic condensers, and oxygen sensors, due to its high melting point, low thermal conductivity, and high mechanical and corrosion resistance (1–4). Because of its high thermal stability, large BET-surface area, and amphoteric properties, zirconia is a promising catalyst support as well (5–7). Copper oxide catalysts supported on Al_2O_3, ZrO_2, and $ZrO_2–Al_2O_3$ with different surface areas have been used for total oxidation of CO (7). It is reported that CuO/ZrO_2 showed better oxidation activity than the other catalysts because of the easy reduction of highly dispersed copper species on ZrO_2 (7). Recently, some efforts have gone into studying the properties of pure and metal-doped zirconia as catalysts for various reactions (8–10). Zamar *et al.* have reported on the complete combustion of methane on zirconia doped with ceria with 50% conversion at 813 K, which is 130 K lower than the combustion temperature on pure ceria (8). According to Keshavaraja and Ramaswamy (9), the introduction of multivalent Mn into the ZrO_2 fluorite lattice accelerated the reaction rate of the complete oxidation of *n*-butane more than single MnO_2, ZrO_2, or the mixed oxides. Choudhary *et al.* further reported (10) that Mn-, Co-, and Fe-stabilized cubic zirconia materials are excellent catalysts for CH_4 combustion with a catalytic activity similar to that of noble metal catalysts. Kundakovic and Flytzani-Stephanopoulos (11) studied the reduction of CuO dispersed on fluorite type oxides, such as La-doped CeO_2 and Y-doped ZrO_2 and observed a clear influence of host oxide on the reduction of copper. Y-doped ZrO_2 containing 15% Cu was the most active catalyst in complete oxidation of methane in the 570 to 825 K temperature range. We report here the preparation of $Cu–ZrO_2$ by a sol–gel procedure, which results in Cu^{2+} ions occupying different sites in stabilized cubic zirconia structure. In the present work, the ^{18}O exchange processes and the oxidation of CH_4 and CO on $Cu–ZrO_2$ are investigated by online mass spectrometry.

[1] To whom correspondence should be addressed. E-mail: dongare@cata.ncl.res.in.

0021-9517/01 $35.00

The results are compared with those obtained from the catalytic oxidation of CH_4 and CO on Cu–ZrO_2.

EXPERIMENTAL

Preparation of Cu–ZrO_2 Samples

Samples of Cu-stabilised zirconia were prepared employing the sol–gel technique. In a typical synthesis, 47 g of zirconium isopropoxide (70 wt.% solution in 1-propanol, Aldrich) was dissolved in 400 ml of dry isopropanol. To this solution, the calculated quantity of $Cu(NO_3)_2 \cdot 3H_2O$ (99.9%, LOBA Chemie) dissolved in 100 ml of isopropyl alcohol was added under constant stirring to obtain a clear, homogeneous solution. Thereafter, a stoichiometric quantity of water and catalytic quantity of hydrochloric acid (0.5 ml of 0.1N HCl) were mixed in 100 ml of isopropanol and introduced to the above solution in order to hydrolyze the zirconium isopropoxide. The mixture obtained was further stirred for 1 h and allowed to stand for 12 h to form a thick transparent gel, which was kept at room temperature for drying. The resulting glassy solid was ground to a fine powder and subsequently heat-treated at different temperatures to study the X-ray structure and phase transformations. The samples were heated for 12 h at 623, for 12 h at 773, and for another 12 h at 873 K. A series of Cu–ZrO_2 samples with a nominal Cu content from 1% up to 33 mol% were prepared by adjusting the appropriate concentrations of $Cu(NO_3)_2 \cdot 3H_2O$ in the initial solutions. Yttrium-stablized zirconia samples with and without Cu were also prepared following a similar sol–gel procedure and employing yttrium nitrate as the yttrium source for comparison.

Selected samples were immersed in 70% nitric acid for 12 h to dissolve extra lattice or dispersed CuO particles, washed with deionized water, dried at 373 K for 8–10 h, and calcined at 873 K for 6 h. The solids were analyzed by XRF and the washings were analyzed by AAS for Cu content.

Sample Characterization

Powder X-ray diffraction analysis was carried out using a Rigaku X-ray diffractometer (Model DMAX IIIVC) equipped with a Ni filtered Cu$K\alpha$ (1.542 Å) radiation and a graphite crystal monochromator. Silicon was used as an external standard. The data were collected in the 2θ range 25–90° with a step size of 0.02° 2θ and counting time of 15 s at each step. The sample was rotated throughout the scan for better counting statistics. The observed inter planar d spacing was corrected with respect to silicon. The unit cell parameters were determined using the corrected d values and then refined using least squares fitting.

Photoemission spectra were recorded on VG Microtech Multilab ESCA 3000 spectrometer using nonmonochromatized Mg$K\alpha$ X-ray source ($h\nu = 1253.6$ eV). Base pressure in the analysis chamber was maintained in the 4–8 $\times$ 10^{-8} Pa range. The energy resolution of the spectrometer was set at 0.8 eV with Mg$K\alpha$ radiation at pass energy of 20 eV. Binding energy (BE) calibration was performed with Au $4f_{7/2}$ core level at 83.9 eV. BE of adventitious carbon (284.9 eV) was utilized for charge correction with Cu–ZrO_2. The error in all the BE values reported here is within ± 0.1 eV.

The surface areas (BET) of the samples were determined after degassing the samples at 573 K and analyzing the N_2 adsorption isotherm at liquid nitrogen temperature (ASAP 2000 system, Micromeritics). The carbon content of the oxides was calculated from the quantity of CO_2 released from the samples during annealing in O_2 at 1323 K. The chemical analysis of the samples was done by atomic absorption and XRF.

Dynamic–Thermal ^{18}O Exchange and Oxidation Measurements

The ^{18}O exchange and oxidation (CO and CH_4) measurements were carried out in a quartz reactor with an online-coupled mass spectrometer. Before starting the reaction, about 300 mg of the sample was heated for 4 h at 573 K and 2 Pa, in order to remove H_2O, CO_2, and other molecules from the surface of the oxide. After cooling down to room temperature, Ar, $^{18}O_2$, and the second reactant (viz., $^{16}O_2$, CO, or CH_4) were introduced in an appropriate ratio into the reaction system. The initial pressure was adjusted to $p_0 =$ 100 Pa, and the quartz reactor was heated to 973 K applying a constant heating rate of $\beta = 10$ K min^{-1}. The variation of the gas phase composition during constant heating was analyzed by a quadrupole mass spectrometer (QMG421I, Pfeiffer Vacuum Gmbh). During the interaction between $^{18}O_2$, $^{16}O_2$, and the solid oxide, diffusion, sorption, and ^{18}O isotope exchange processes may take place according to the following schemes:

Homogeneous ^{18}O isotope Exchange,

$$^{18}O_{2(g)} + {}^{16}O_{2(g)} \rightarrow 2{}^{16}O{}^{18}O_{(g)}, \qquad [1]$$

partially heterogeneous ^{18}O isotope exchange,

$$^{18}O_{2(g)} + {}^{16}O_{(s)} \rightarrow {}^{16}O{}^{18}O_{(g)} + {}^{18}O_{(s)}, \qquad [2]$$

completely heterogeneous ^{18}O isotope exchange,

$$^{18}O_{2(g)} + 2{}^{16}O_{(s)} \rightarrow {}^{16}O_{2(g)} + 2{}^{18}O_{(s)}. \qquad [3]$$

From the occurrence of the individual processes and the onset temperatures, conclusions can be drawn on temperature regions of enhanced oxygen mobility and activity to promote homogeneous or heterogeneous redox reactions. The measuring principle and the theoretical background of the ^{18}O isotope exchange measurements are described

in detail elsewhere (12, 13). In a similar manner, the oxidation of CO or CH_4 by $^{18}O_2$ can be investigated. For that purpose, the reaction gas mixture ($p_0 = 100$ Pa) was introduced into the quartz finger and the reaction system was heated to 873 K. The onset of the oxidation reaction and the oxidation products distribution were determined to draw conclusions on the mechanism of the catalytic process.

Catalytic Oxidation of CH_4

The catalytic oxidation of CH_4 was performed in an upflow, fixed-bed quartz reactor. Approximately 300 mg of the ground oxide was pressed in the form of pellet. The pellet was crushed to obtain the catalyst in the granular form (mesh size 0.5–1 mm) and was preheated for 1 h at 723 K in N_2 flow (10 ml min^{-1}). After cooling down to 523 K, the sample was exposed to the reaction gas mixture of O_2 (48 ml min^{-1}) and CH_4 (12 ml min^{-1}) at atmospheric pressure and at a residence time of 0.25 s (gas hourly space velocity of 15000 h^{-1}). After 20 min., the gas composition at the reactor exit was determined by an online gas chromatograph (Shimadzu 17A) with thermal-conductivity detector (column: C molecular sieve, i.d. 3 mm, length: 2 m). The conversion of methane was calculated in terms of CO_2 formed. The catalyst was tested with ascending and descending temperature to study the light-off temperature and catalyst deactivation. The catalytic activity was also studied at various lower residence time to study the mass transfer limitations.

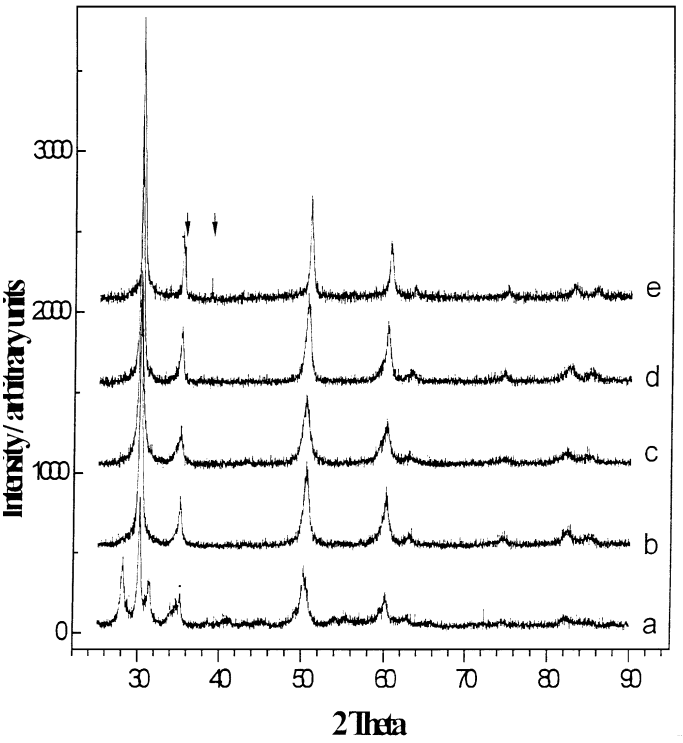

FIG. 1. Powder XRD profiles of ZrO_2 (curve a) and Cu–ZrO_2 samples containing 5, 10, 20, and 25 mol% Cu in ZrO_2 prepared by sol–gel procedure and calcined at 873 K (curves b to e, respectively).

RESULTS AND DISCUSSION

Sample Characterization

Cu–ZrO_2 samples with a copper content of 1–20 mol% were light green to greenish black in color. These samples prepared by the sol–gel method were found to be very appropriate for ^{18}O exchange and related measurements. The residual carbon content in all Cu–ZrO_2 samples was low and in the range of 0.10 to 0.23%, so that the combustion of organic impurities does not interfere with the isotope exchange processes in ^{18}O exchange experiments (Table 1). The BET surface areas of the samples (calcined at 873 K) were in the range of 2 to 8 $m^2 g^{-1}$. Since different types of Cu species exist in these samples, there is no monotonic decrease or increase in the surface area of the samples with increasing Cu content. The multiple XRD patterns of representative samples are given in Fig. 1 (see lines a–e). Unlike

TABLE 1

XRD, Carbon Content, BET Surface Area, and Onset Temperature of Completely Heterogeneous ^{18}O Exchange of Cu–ZrO_2 with Different Nominal Cu Contents (mol%)[a]

Cu mol%	XRD phases	Carbon content wt%	Lattice parameter *a*, Å	S_{BET}/ $m^2 g^{-1}$	T_{ex}/K
0.00	Cubic ZrO_2 + monoclinic (traces)	0.10	5.09	40	No exchange
2.00	Cubic ZrO_2	0.15	5.085	2.0	738
5.00	Cubic ZrO_2	0.11	5.084	4.0	688
10.00	Cubic ZrO_2	0.21	5.077	8.0	633
20.00	Cubic ZrO_2	0.11	5.065	6.0	593
25.00	Cubic ZrO_2 + CuO (traces)	0.17	5.058	3.0	593
33.00	Cubic ZrO_2 + CuO	0.23	—	4.0	608
Y_2O_3–ZrO_2 (8:92 mol%)	Cubic ZrO_2	0.37	—	17	—
Cu–Y_2O_3–ZrO_2 (17:8:75)	Cubic ZrO_2	0.255	—	31	—

[a] Pure ZrO_2 was calcined at 723 K; all Cu–ZrO_2 samples were calcined at 873 K.

that in other techniques, pure zirconia prepared by sol–gel method and calcined at 723 K is predominantly in a metastable cubic structure with a small amount of monoclinic phase, having a higher surface area of 40 $m^2\ g^{-1}$ (Fig. 1, line a). When it was further heated at 873 K, it transforms to a more stable monoclinic phase. The Cu–ZrO_2 samples with Cu content in the range 2–20 mol% exhibit the cubic fluorite structure ($2\theta = 30.4°, 35.4°, 50.7°, 60.4°, 63.2°, 74.8°, 82.6°$, and $85.4°$) even after calcination at higher temperatures (873 K) (Fig. 1, lines b–d). The XRD pattern of the sample with 25 mol% of Cu reveals the presence of some copper oxide phase (Fig. 1, line e, very weak XRD peaks at $2\theta = 35.6°$ and $38.8°$ shown with arrows). This study indicates that Cu content from 2–20 mol% in Cu–ZrO_2, stabilizes zirconia in the cubic fluorite structure. The lattice parameter decreases from 5.09 (for pure zirconia) to 5.058 Å as the Cu content increases from 0 to 25 mol%.

Figure 2 shows the variation of the cubic lattice parameter, which is fairly linear with the copper content in ZrO_2. Also shown in Fig. 2 are the calculated lattice parameters for the known molar concentrations of copper in ZrO_2, assuming substitution of Zr^{4+} (ionic radius = 0.84 Å) in eightfold coordination by smaller Cu^{2+} ions (ionic radius = 0.72 Å), in sixfold coordination in the cubic lattice. It is seen that up to 2% of Cu, the experimental lattice parameter values agree with the calculated values. This indicates the substitution of Zr^{4+} by Cu^{2+} ions in the lattice. As the copper content increases, more Cu^{2+} ions may go into the lattice, but the decrease in lattice parameter does not match with the theoretical values beyond about 2 mole% Cu in ZrO_2. On a rough approximation, only about one half of the input Cu probably goes into the lattice, because 5, 10, 20 mole% (input) Cu samples give lattice parameters equivalent to the calculated values for 2.5, 5, and 10% Cu, respectively. In the Cu concentration range of 5 to 20 mole% in ZrO_2, even though the XRD patterns do not reveal the presence of separate CuO phase, it is likely that Cu^{2+} ions exist in different locations of the Cu–ZrO_2 samples. Apart from substitutional positions, Cu^{2+} ions may exist on the surface or subsurface layers, coordinated to the surface oxide ions, as isolated species, or they may exist as very small crystallites of CuO (which are XRD amorphous). The Cu^{2+} ions in the substitutional positions of cubic ZrO_2 will create oxide ion vacancies balancing the charge. As the Cu content increases to 25 mole%, it is possible that smaller crystallites of CuO agglomerate to bigger crystals and is seen as bulk CuO phase in the XRD profile (Fig. 1, line e). It may be noted that only a few ppm of Cu could be extracted by an acid treatment from samples containing Cu in the range of 2 to 20 mole%. This suggests that almost all Cu is well bound to the oxygen of ZrO_2 either in the lattice or strongly bound to the surface or subsurface layers of cubic ZrO_2 (11). The regression coefficient R, from the least square fit is -0.9973 for the experimental data, which is extremely satisfactory. The standard deviation of the lattice parameters for all the samples varied from 0.0013 to 0.0028, which is shown in Fig. 2.

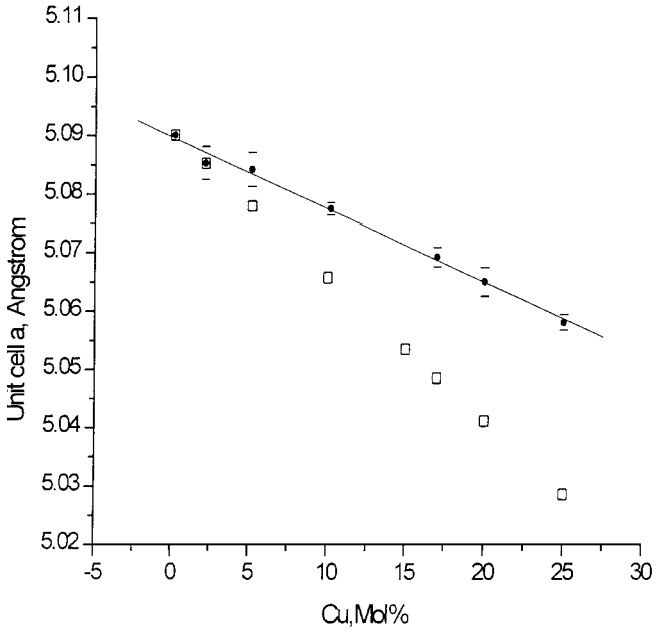

FIG. 2. Variation in cubic unit-cell parameters of Cu–ZrO_2 samples with an increase in copper content. Experimental and theoretical data points are denoted by circles and squares, respectivley.

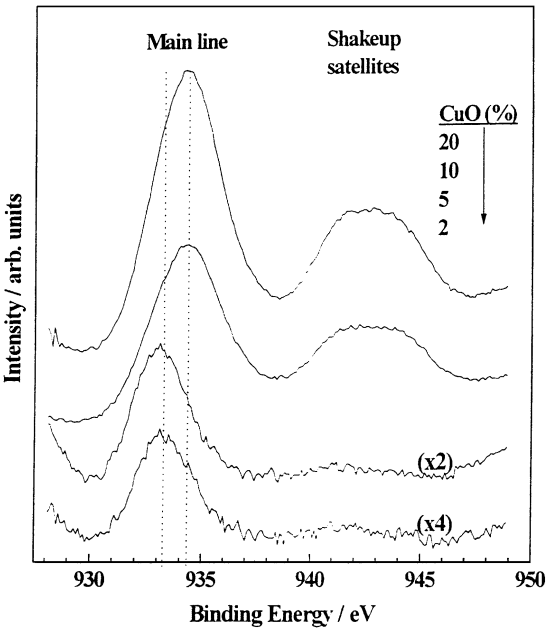

FIG. 3. X-ray photoemission spectra for Cu–ZrO_2 samples with various copper loading recorded at room temperature with Mg $K\alpha$ radiation.

The Cu–ZrO_2 samples were further characterized by X-ray photoelectron spectroscopy (XPS) to shed some light on their electronic structure. Figure 3 shows the photoemission spectra from Cu $2p_{3/2}$ core level at different copper loading.

An interesting observation is that at low copper loadings (≤5 mol%), there is only one peak at a BE of 933.3 eV without any satellite at higher BE. However, at Cu levels of ≥10 mol%, there is a clear broadening observed with main line and is shifted to higher BE at 934.4 eV. Additionally, it shows a strong satellite in the energy range between 938 and 947 eV. The BE of the main line clearly indicates that the oxidation state of copper species is essentially Cu (II) and it is in good agreement with the values reported in the literature (14–17).

The absence of satellite peaks in Cu–ZrO_2 samples at Cu loading levels of ≤5 mol% clearly indicates that there is a very good interaction in terms of charge transfer from nearby oxygen ligands to copper and hence the BE of main line is lower than the BE of pure CuO, which appears at 934.1 eV (15). The low BE associated with this peak also hints that it might be associated with the holes created by oxygen vacancies in the ZrO_2 lattice. This copper species is attributed to the copper inside the ZrO_2 lattice and most likely one of the catalytically active sites for the oxidation reaction. The intensity of this peak increases with copper loading. However, there is a high BE feature observed at 934.4 eV with satellite feature and its intensity also increases from 10 mol% of Cu and above. This feature is essentially the same as that of CuO, except for somewhat higher BE at 934.4 eV and is attributed to CuO dispersed in the lattice. Acid leaching of the above samples does not remove any extra lattice copper, and this clearly suggests that the above CuO species could be interfaced with the ZrO_2 lattice. The extra features seen in samples containing ≥10 mol% Cu are completely missing in samples with ≤5 mol% Cu. This clearly indicates that there may not be any extra lattice CuO in samples containing ≤5 mol% Cu, at least on the surface.

The XPS results thus support the findings from XRD. Both techniques show that about half of the input copper goes into the lattice and the remaining should be present as surface and/or subsurface cupric oxide species. There are, however, some differences between the observations from XRD and XPS, which could be attributed to the different surface sensitivity of XPS and XRD. For examples, XPS data reveal the presence of distinct surface CuO species in samples containing 10 mol% Cu in ZrO_2. These are presumably amorphous CuO and not detected by XRD.

^{18}O Isotope Exchange on Cu–ZrO_2

The processes occurring during the constant heating of Cu–ZrO_2 in a $^{18}O_2$: $^{16}O_2$ ratio of 2 : 1 gas atmosphere (p_0 = 100 Pa) are exemplified on Cu-stabilized zirconia samples with CuO content of 10 mol% (Fig. 4). At 473 K, $^{16}O_2$ and $^{18}O_2$ enter the solid occupying the oxygen vacancies caused by the thermal pretreatment (573 K, 4 h, 2 Pa) of the samples. Above 573 K, small quantities of CO_2 and H_2O are released which could not be completely removed during the pretreatment procedure. Complete removal of carbon compounds and OH-groups from the solid before starting

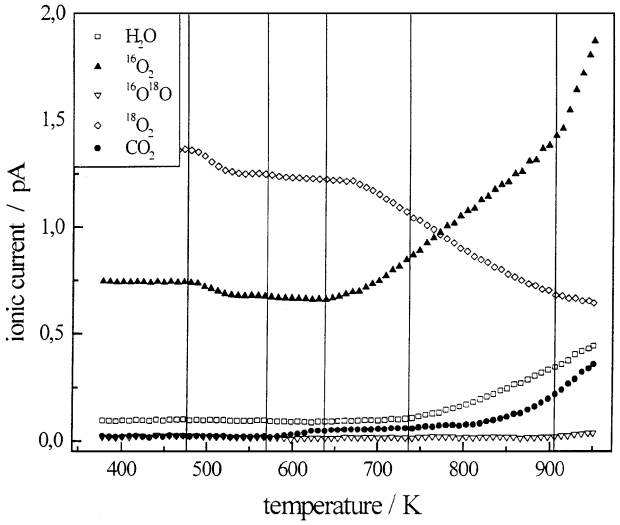

FIG. 4. ^{18}O isotope exchange reaction on cubic Cu–ZrO_2 with 10 mol% Cu content at p_O = 100 Pa (60 Pa $^{18}O_2$, 30 Pa $^{16}O_2$, 10 Pa Ar).

the measurement is impossible, since the temperature and pressure of the pretreatment must be chosen in such a way that undesired reduction processes are avoided. Therefore, especially large surface area samples prepared from organic precursors may release CO_2 and H_2O above the pretreatment temperature. With all Cu–ZrO_2 samples, however, the quantities of CO_2 and H_2O desorbed during the measurements did not affect the ^{18}O-exchange process. At 633 K, the $^{18}O_2$ content decreases and $^{16}O_2$ is formed while the partial pressure of $^{16}O^{18}O$ remains constant up to 973 K. Hence, the completely heterogeneous oxygen exchange (Eq. [3]) is the only isotope exchange process occurring on cubic Cu–ZrO_2 under the above measuring conditions. Such a behavior is different from that of other Cu oxides with smaller BET-surface areas. During ^{18}O isotope exchange measurements on commercial CuO ($S_{BET} < 1\ m^2\ g^{-1}$), considerable quantities of $^{16}O^{18}O$ were formed by homogeneous (Eq. [1]) and partially heterogeneous exchange (Eq. [2]). Moreover, traces of $^{16}O^{18}O$ were detected during the measurements on high-Cu containing samples with CuO impurities. Obviously, the ^{18}O exchange rate on Cu–ZrO_2 with Cu^{2+} in lattice and surface sites is so high that the heterogeneous exchange of both ^{18}O atoms of an $^{18}O_2$ molecule is favored over the desorption of an $^{16}O^{18}O$ molecule. The onset temperature of the completely heterogeneous ^{18}O exchange, T_{ex}, strongly depends on the Cu content of Cu–ZrO_2 (see Table 1). T_{ex} decreases with Cu content and passes through a minimum at Cu content of 20 mol%, which is the last oxide in the series without bulk CuO impurities. The occurrence of bulk-like CuO leads to a slight reduction in the ^{18}O-exchange activity of Cu–ZrO_2.

CH_4 Combustion on Cu–ZrO_2

The catalytic activity of Cu–ZrO_2 samples in complete CH_4 combustion was studied after calcining the ground

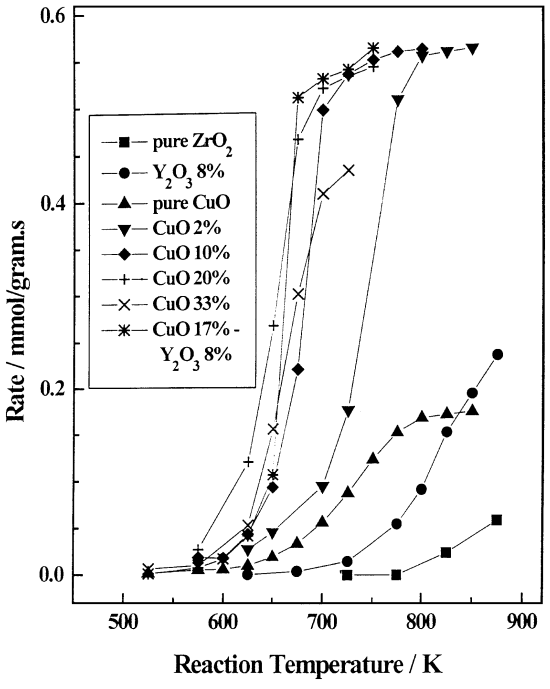

FIG. 5. Catalytic activity of ZrO_2, CuO, Y_2O_3–ZrO_2, CuO–Y_2O_3–ZrO_2, and CuO–ZrO_2 for methane oxidation at a residence time of 0.25 s.

powder at 873 K in a quartz reactor. Figure 5 depicts the catalytic activity for the complete oxidation of CH_4 between 573 and 873 K for Cu–ZrO_2 and the single metal oxides (ZrO_2 and CuO) as reference. Pure zirconia and CuO are not as active and only 22% conversion was seen at 873 K. All tested cubic Cu–ZrO_2 catalysts proved to be active, leading to a total conversion of CH_4 within 673 and 773 K. The addition of Cu shifts the light-off curves to lower temperatures. In every case, CO_2 was the sole product and no carbon monoxide or partial oxidation products were detected during oxidation. For the individual catalysts, the temperature range between an appreciable methane conversion (10–15%) and nearly complete conversion of CH_4 (96–98%) was found to be quite narrow, never exceeding 100 K. Sample containing 20 mol% of Cu showed the best catalytic performance, with 95% conversion at 673 K, among the series under study. The effect of the specific surface area on the catalytic performance is of secondary importance, considering the fact that all the Cu-samples have almost similar, low surface areas. A steady increase in catalytic activity of Cu–ZrO_2 samples with Cu content up to 20 mol% clearly shows that the catalytic activity is related to the Cu species present in the lattice positions as well as on the surface/subsurface layers of cubic ZrO_2. The catalytic activity of Cu–ZrO_2 (Cu content 20 mol%) sample was also studied at lower residence time than 0.25 s and there was no appreciable change in the catalytic activity. The steep increase in the conversion of methane after light-off is normally associated with auto-thermal oxidation due to exothermicity of the reaction. With a very small quantity of the catalyst in a microreactor, a temperature rise of about 5 K between the thermocouple inside and outside the reactor was noticed. In this region of autothermal oxidation, the influence of residence time on activity is not perceived to be any different and is probably limited by mass transfer.

The catalytic activity of yttrium-stabilized ZrO_2 containing an equivalent amount of copper is apparently higher than that of corresponding Cu–ZrO_2. The light-off temperature was 650 K for yttrium-stabilized ZrO_2 with copper, which was lower than for Cu–ZrO_2 (673 K) (Fig. 5). However, without Cu the yttrium-stabilized ZrO_2 showed a very low activity. It is also interesting to note that yttrium-stabilized ZrO_2 (cubic) was comparatively more active than pure ZrO_2 (monoclinic). The higher catalytic activity of the Cu–ZrO_2 with 20 mol% in the system under study is attributed to maximum amount of copper in substitutional position and the resulting oxygen vacancies. The Cu in the lattice position seems to be an active site for redox reaction, and oxygen vacancies enhance the catalytic activity because of the higher oxygen mobility in cubic zirconia. The higher activities of yttrium zirconia as compared to pure zirconia (Fig. 5) illustrate the influence of oxygen vacancies and their mobility on catalytic activity. The catalytic activity of Cu–ZrO_2 reported here is somewhat comparable to that reported by Kundakovic *et al.* (11), where Cu was dispersed on the surface of zirconia. In fact, in both the cases, the 20% Cu catalysts have similar light-off temperatures, even though there is a large difference in the space velocities (80,000 h^{-1} vs 15,000 h^{-1}). However, part of the Cu^{2+} ions in the present system are in the substitutional position because of the sol–gel method of preparation. The sol–gel method of preparation has well-known advantages over coprecipitation method and yielded Cu–ZrO_2 samples with stabilized cubic structure. The catalytic activity of Cu–ZrO_2 in complete oxidation of methane was also higher than that of substituted perovskites (18) and perovskite-based catalysts (19). The enhancement in catalytic activity in total oxidation using perovskite (ABO_3) was correlated with the defect structure and oxygen vacancies created because of substitution of *A* and/or *B* site cation. Similar enhancement in catalytic activity in complete oxidation of *n*-butane using Mn stabilized zirconia has been reported by Keshavaraja and Ramaswamy (9). The activity for methane oxidation increases until bulk-like CuO is formed on the surface of the solid. Although the observed activity is much higher than that of mixed-metal oxides with zirconia as support and other metal oxides (5–8, 10), the performance can even be improved by optimizing the calcination conditions.

The light-off temperatures for 50% conversion of CH_4, $T_{50\%}$, fit in a good manner with the results obtained from the ^{18}O exchange measurements (Fig. 6). The shape of the curves of T_{50} and T_{ex} with increasing Cu content is remarkably identical. The temperature difference between

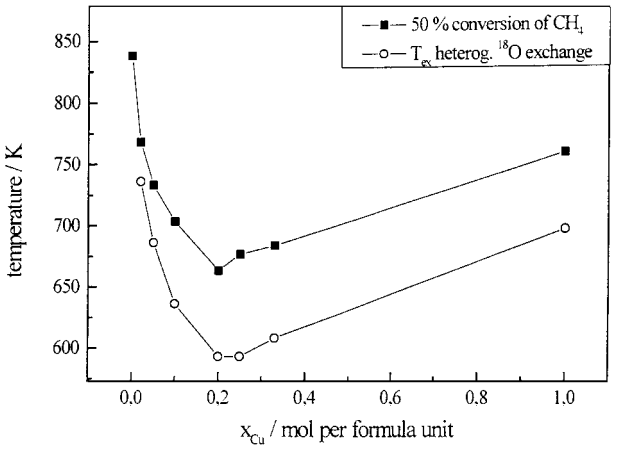

FIG. 6. Correlation between light-off temperature ($T_{50\%}$) of CH_4 combustion and onset temperature (T_{ex}) of completely heterogeneous ^{18}O exchange as a function of Cu content in cubic ZrO_2 ($Cu_xZr_{1-x}O_2$).

the curves can easily be explained by the fact that T_{ex} is the onset temperature for exchange ($p \sim 10^2$ Pa), whereas T_{50} is the temperature required for 50% conversion of CH_4 at $p \sim 10^5$ Pa. From Fig. 6, it can be concluded that both the catalytic combustion of CH_4 and the oxygen isotope exchange occur via a completely heterogeneous mechanism. Even though such a correlation does not mechanistically create a correct picture, it is interesting to see the influence of Cu concentration on ^{18}O exchange capacity and methane oxidation follow a similar trend. This conclusion is supported by the results of CH_4 oxidation at 100 Pa of $^{18}O_2$ (Fig. 7). After the adsorption of $^{18}O_2$ at 483 K, a number of different processes start to occur at 588 K. The $^{16}O_2$ content increases due to completely heterogeneous ^{18}O exchange. Simultaneously, the CH_4 content decreases while CO_2 (44 AMU) and H_2O (18 AMU) are formed. Obviously, CH_4 is oxidized, but

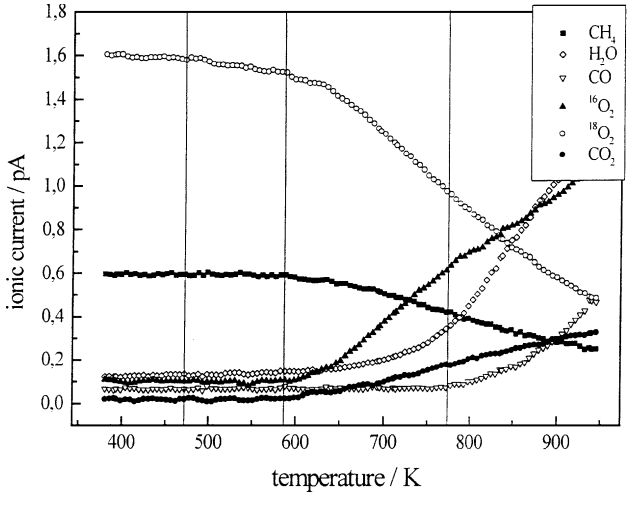

FIG. 7. Oxidation of CH_4 by $^{18}O_2$ on cubic Cu–ZrO_2 (10 mol% Cu) at $p_O = 100$ Pa (63 Pa $^{18}O_2$, 27 Pa CH_4, 10 Pa Ar).

not by a homogeneous reaction between gaseous reactants on the catalyst surface. The absence of ^{18}O-containing oxidation products ($C^{18}O_2$, $C^{16}O^{18}O$, $H_2{}^{18}O$) clearly suggests that ^{16}O from the solid acts as oxidizing agent in a heterogeneous catalytic mechanism.

Very similar results were obtained from the oxidation of CO by $^{18}O_2$ at $p = 100$ Pa. Here, CO is oxidized to CO_2 (44 AMU), exclusively, at an onset temperature of 393 K. Obviously, ^{16}O from the solid is released accompanied by the reduction of active Cu^{2+} species, even at low temperatures, depending on the reduction potential of the reactants. The completely heterogeneous mechanism of ^{18}O isotope and oxidation reactions can be described by following equations (isotope exchange):

$$2^{16}O^{2-}_{(s)} \rightarrow [^{16}O_{2(g)} + 4e] \rightarrow {}^{16}O_{2(g)} + (V_OV_O)_s$$

$$^{18}O_{2(g)} + (V_OV_O)_{(s)} \rightarrow [2^{18}O_{(g)} + 4e] \rightarrow 2^{18}O^{2-}_{(s)}$$

Catalytic CH_4-Combustion

From these results, the catalytic combustion of CH_4 over Cu-ZrO_2 catalyst can be described as follows. When ^{18}O and CH_4 are passed over the catalyst, initially they are adsorbed on the catalyst surface. The $^{16}O^{2-}$ from the bulk of catalyst reduce the Cu^{2+} ions in the lattice or surface/subsurface layers of ZrO_2 to Cu^{1+} and form an active oxygen, which oxidizes CH_4 to CO_2, and an oxygen vacancy is created in the zirconia lattice. ^{18}O from the surface of the catalyst oxidizes the Cu^{1+} to Cu^{2+} ions, diffuses into the lattice as $^{18}O^{2-}$, and occupies an oxygen vacancy site. The oxygen vacancies in the zirconia lattice facilitate the diffusion of $^{18}O^{2-}$ and $^{16}O^{2-}$ because of higher oxygen mobility in zirconia lattice, thereby enhancing the catalytic activity. The possible reaction mechanism can be given as follows:

$$CH_{4(g)} + {}^{18}O_{2(g)} \rightarrow CH_{4(ads)} + {}^{18}O_{2(ads)}$$

$$4^{16}O^{2-}_{(s)} \rightarrow 4^{16}O^* + 8e + 4Vo$$

$$8Cu^{2+} + 8e \rightarrow 8Cu^{1+}$$

$$CH_{4(ads)} + 4^{16}O^* \rightarrow CO_{2(g)} + 2H_2O_{(g)}$$

$$8Cu^{1+} \rightarrow 8Cu^{2+} + 8e$$

$$2^{18}O_{2(ads)} + 8e \rightarrow 4^{18}O^{2-}_{(s)}$$

$$4^{18}O^{2-}_{(s)} + 4(V_O)_s \rightarrow 4^{18}O^{2-}_{(s)},$$

where, V_O represents the oxygen vacancies and O^* the active oxygen.

Such a catalytic mechanism is usual for transition-metal oxides and agrees with the findings of Choudhary *et al.* (10), who observed a key role of lattice oxygen during the combustion of CH_4 on Mn-stabilized zirconia. Since pure ZrO_2 is a poor catalyst for ^{18}O exchange and oxidation processes, it is evident that the oxidizing O from the bulk is connected

with active Cu^{2+} centers. The role of Cu in Cu–ZrO_2 is twofold, creation of oxygen vacancies and a redox center. The oxygen vacancies increase the oxygen mobility and facilitate the oxygen diffusion increasing the catalytic activity.

CONCLUSIONS

A series of samples of Cu-stabilized cubic zirconia, Cu–ZrO_2 with Cu content from 1 to 33 mol%, was prepared by sol–gel procedure. The decrease in unit-cell values with increase in copper concentration supports the incorporation of copper in the lattice position. XPS study of these samples showed that Cu is essentially in Cu^{2+} oxidation state and incorporates into the ZrO_2 lattice up to 5 mol%. Approximately half of the input copper goes into the lattice and the remainder stays as extra lattice copper in samples with Cu above 5 mol%, supporting the findings from XRD. The surface areas of Cu–ZrO_2 samples calcined at 873 K varied from 2 to 8 m^2/g. Catalytic studies, ^{18}O isotope exchange, and oxidation experiments revealed appreciable catalytic activity of the samples depending on the nominal Cu content. Both exchange and oxidation reactions occur via a completely heterogeneous mechanism with the release of ^{16}O from the solid phase as the initial reaction step. The bulk oxygen associated with the oxidation is connected with Cu^{2+} species on lattice/surface sites. These Cu species are easily reduced and reoxidized in a catalytic cycle, thus acting as active centers for the completely heterogeneous ^{18}O exchange as well as for oxidation processes. The incorporation of redox Cu^{2+} active species into the structure of cubic ZrO_2 combined with oxygen mobility due to oxygen vacancies leads to the formation of catalysts, which are superior to either CuO or ZrO_2, or CuO supported on ZrO_2.

ACKNOWLEDGMENTS

The authors gratefully acknowledge the financial support from the Volkswagen-Stiftung (project I/73 506) enabling the scientific cooperation between the two institutions. E.K. and S.S. are obliged to the Deutsche Forschungsgemeinschaft (Ke 489/-11-2) for promoting this work.

REFERENCES

1. Mazdiyasni, K. S., Lynch, C. T., and Smith, J. S., *J. Am. Ceram. Soc.* **50**, 532 (1967).
2. Subbarao, E. C., "Solid Electrolytes and Their Applications." Plenum Press, New York, New York 1980.
3. George, A. M., Mishra, N. C., and Jayadevan, N. C., *J. Mater. Sci. Lett.* **23**, 404 (1992).
4. Chirino, A. M., and Sproule, R. T., *Am. Ceram. Soc. Bull.* **59**, 604 (1980).
5. Tanabe, K., and Yamaguchi, T., *Catal. Today* **20**, 185 (1994).
6. Okamoto, Y., Gotoh, H., Aritani, H., Tanaka, T., and Yoshida, S., *J. Chem. Soc. Faraday Trans.* **93**, 3879 (1997).
7. Zhou, R. X., Jiang, X. Y., Mao, J. X., and Zheng, X. M., *Appl. Catal. A* **162**, 213 (1997).
8. Zamar, F., Trovarelli, A., de Leitenburg, C., and Dolitti, G., *J. Chem. Soc. Chem. Commun.* 965 (1995).
9. Keshavaraja, A., and Ramaswamy, A. V., *Appl. Catal. B* **8**, L1 (1996).
10. Choudhary, V. R., Uphade, B. S., Pataskar, S. G., and Keshavaraja, A., *Angew. Chem.* **108**, 2538 (1996).
11. Kundakovic, L. J., and Flytzani-Stephanopoulos, M., *Appl. Catal. A* **171**, 13 (1998).
12. Kemnitz, E., Menz, D. H., Stoecker, C., and Olesch, T., *Thermochim. Acta* **225**, 119 (1993).
13. Kemnitz, E., Galkin, A. A., Olesch, T., Scheurell, S., and Mazo, G. N., *J. Thermal Anal.* **48**, 997 (1998).
14. Van der Lann, G., Westra, C., Haas, C., and Sawatzky, G. A., *Phys. Rev. B* **23**, 4369 (1981).
15. Allan, K., Campion, A., Zhou, J., and Goodenough, J. B., *Phys. Rev. B.* **41**, 11572 (1990).
16. Wagner, C. D., Riggs, W. M., Davis, L. E., Moulder, J. F., and Muilenberg, G. F., "Handbook of X-Ray Photoelectron Spectroscopy." Perkin–Elmer Corporation, Physical Electronics Division, Eden Prairie, MN, 1979, and references therein.
17. Larsson, S., and Braga, M., *Chem. Phys. Lett.* **48**, 596 (1977).
18. Arai, H., Yamade, T., Eguchi, K., and Seiyama, T., *Appl. Catal.* **26**, 265 (1986).
19. Cimino, S., Lisi, L., Pirone, R., Russo, G., and Turco, M., *Catal. Today* **59**, 19 (2000).